Thin-Walled Structures 189 (2023) 110892

Contents lists available at ScienceDirect

Thin-Walled Structures

journal homepage: www.elsevier.com/locate/tws

Full length article

Experimental and numerical study on crashworthiness of bionic hedgehog spine thin-walled structures

Bin Liu [a,b], Xianghong Xu [a,*]

[a] The state key laboratory of nonlinear mechanics, Institute of Mechanics, Chinese Academy of Sciences, Beijing, 100190, China
[b] School of Engineering Sciences, University of Chinese Academy of Sciences, Beijing, 100049, China

ARTICLE INFO

Keywords:
Thin-walled structure
Impact compression
Crashworthiness
Bionic design
Hedgehog spine

ABSTRACT

Natural impact-resistant biomaterials, with ingenious and exquisite geometric configurations, have resistance to external impact, and thus provide a perfect bionic example for the optimization design and crashworthiness improvement of new thin-walled structures. Based on the configuration characteristics of hedgehog spine, this paper designed the bulkheaded hedgehog spine thin-walled structure and studied the dynamic behavior of thin-walled structures under axial and oblique impact compression by combining 3D metal printing, quasi-static compression test and finite element simulation. The results show that the combined effect of the ribs, inner walls and bulkheads of the bulkheaded hedgehog spine thin-walled structure effectively improves its deformation coordination ability and crashworthiness. The specific energy absorption of the bulkheaded hedgehog spine thin-walled structure under axial or oblique impact is about 4.1, 2.1 and 1.4 times that of the single-wall cylinder, spider web and simplified hedgehog spine thin-walled structures, respectively.

1. Introduction

With high specific energy absorption and strength, thin-walled structures can be used as efficient energy absorption devices [1,2]. Upon impact, thin-walled structures can, through irreversible plastic deformation, absorb most of the kinetic energy of the impactor [3,4]. In order to effectively reduce the damage of collision to drivers and key components, thin-walled structures have been widely used in engineering equipment to improve the anti-impact performance thereof, which may be represented by the buffer tube at the head or the carriage connection of high-speed train [5], the energy absorption box at the front of the car [6], the landing gear on the bottom of planetary lander [7] and helicopter [8], etc. Energy-absorption devices in actual service may withstand the impact of axial or oblique load [9,10]. The deformation modes and mechanisms of thin-walled structures are different at different impact angles, making the oblique crashworthiness of thin-walled structures lower than the axial crashworthiness thereof [11]. Therefore, improving the crashworthiness of thin-walled structures at different impact angles has attracted extensive attention of researchers.

For single-wall structures with a regular polygon section, the energy absorption of the structures is directly proportional to the number of polygon sides, indicating that among all these structures, the single-wall cylinder structure performs best in energy absorption [12]. The section design of complex polygons such as star [13] or non-convex polygons [14,15], can enhance the corner constraint of thin-walled structures. The improvement in the corner constraint makes such structures undergo more uniform progressive folding deformation upon axial impact. Therefore, such structures have higher crashworthiness than those with a regular polygon section, premised on the same number of polygon sides.

For single-wall cylinder with uniform wall thickness, the reduction of radius–thickness ratio increases specific energy absorption but reduces crushing force efficiency [16]. While for bamboo-like single-wall cylinder with gradient wall thickness (Fig. 1(a)), specific energy absorption and crushing force efficiency can be improved at the same time, since the number of folds thereof is higher than that of single-wall cylinder with uniform wall thickness during axial impact [17]. In addition, the design of double cylinder walls with approximate diameters can enhance the mutual extrusion of both the inner and outer walls in the process of folding, making the specific energy absorption of double-wall cylinder [18] and double-wall square cylinder [19] higher than that of corresponding type of single-wall cylinders.

Imitating the solid bulkhead between bamboo joints, the addition of bulkheads in the non-convex 20-edge single-wall structure (Fig. 1(b)) can improve the specific energy absorption, mean crushing force, peak crushing force and crushing force efficiency of 114%, 133%, 42% and 32% respectively [14]. The specific energy absorption and crushing force efficiency of a double-wall cylinder can be increased to varying degrees by incorporating 5 ribs with a conical section that simulate the raptorial legs of mantis shrimp [26], 4 ribs with a X-shaped section that

* Corresponding author.
E-mail address: xxh@lnm.imech.ac.cn (X. Xu).

https://doi.org/10.1016/j.tws.2023.110892
Received 16 February 2023; Received in revised form 11 May 2023; Accepted 21 May 2023
Available online 18 June 2023
0263-8231/© 2023 Elsevier Ltd. All rights reserved.

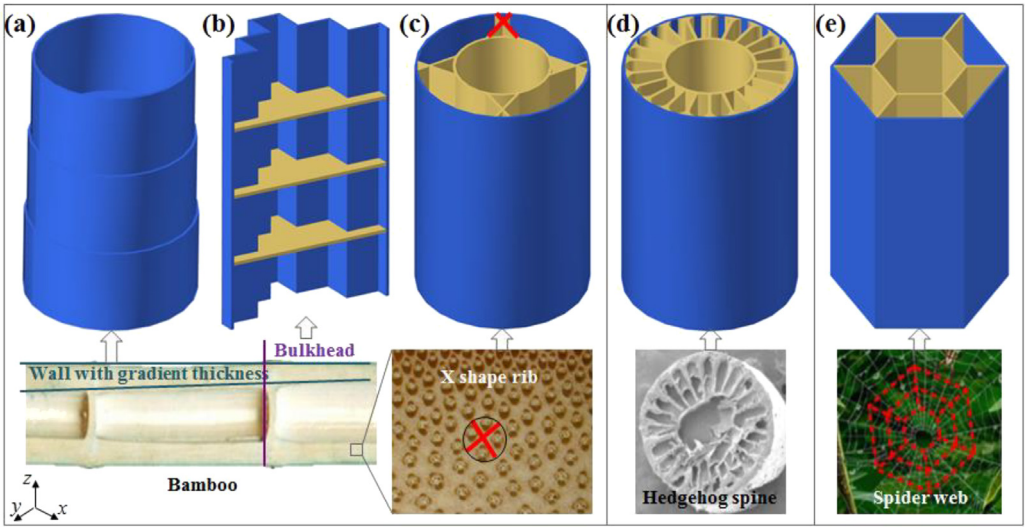

Fig. 1. Biomaterials and biomimetic thin-walled structures. (a) Bamboo-like single-wall cylinder with gradient wall thickness [17,20]; (b) Non-convex 20-edge single-wall structure with bulkheads [14]; (c) Double-wall cylinder with X-shaped ribs [21,22]; (d) Hedgehog spine-like double-wall structure [23,24]; (e) Spider web-like double-wall structure [25].

simulate bamboo (Fig. 1(c)) [21], or 22 ribs with a rectangular section featuring transitional circular arc connection with the outer wall that simulate the cross section of hedgehog spine (Fig. 1(d)) [23]. The specific energy absorption of a double-wall regular hexagonal structure incorporating ribs with a rectangular section that simulates spider web is higher than that of a single-wall regular hexagonal structure (Fig. 1(e)) [25].

The essence of improving the axial crashworthiness by changing the configuration of section or increasing the number of cylinder walls is to make thin-walled structures fold stably in the process of deformation and enhance the interaction between the inner and outer cylinder walls, so as to enlarge the areas for bearing and storage of energy through deformation. As for double-wall cylinders, the aforesaid two improvement mechanisms can be fulfilled at the same time by incorporating an excellent design of ribs with a bionic section between the two walls. Moreover, the bulkhead design can significantly improve the axial crashworthiness of thin-walled structures by enhancing lateral constraint to prevent uneven expansion and mitigate material failure.

The bionic design above can also improve the oblique crashworthiness of thin-walled structures to varying degrees [11,26–28]. The oblique crashworthiness of single-wall cylinder with gradient wall thickness is higher than that of single-wall cylinder with uniform wall thickness, and the specific energy absorption and peak crushing force thereof have the largest percentage improvement at an impact angle of 10° [11]. The crushing force efficiency of both double-wall regular hexagonal structure [27] and double-wall cylinder structure [28] connected by ribs with a rectangular section are higher than those of the single-wall versions thereof at each impact angle. The specific energy absorption thereof have the largest percentage improvement at an impact angle of 10°, respectively 12% and 55% higher than those of the single-wall versions thereof. The oblique crashworthiness of the double-wall cylinder connected by ribs with a rectangular section is higher than that of the single-wall cylinder. The specific energy absorption, peak crushing force and crushing force efficiency thereof have the largest percentage improvement at an impact angle of 20°, respectively 224%, 31% and 43% higher than those of the single-wall cylinder thereof [26].

In this paper, the bulkheaded hedgehog spine thin-walled structure will be created by simulating the configuration characteristics of the cross and longitudinal sections of hedgehog spines. Then the aforesaid structure will be compared with the single-wall cylinder structure, the spider web structure and the simplified hedgehog spine structure described in relevant literatures in terms of axial and oblique crashworthiness, by using the 3D metal printing technology, the quasi-static compression test and the finite element simulation. The mechanism for comprehensively improving the crashworthiness of the hedgehog spine thin-walled structure by the configuration design of rib and bulkhead will be discussed by comparing the deformation modes and energy storage of the above-mentioned four bionic thin-walled structures at different impact angles, with a view to providing new ideas for the design of new energy-absorption devices.

2. Experiment and finite element simulation

2.1. Thin-walled structure model

Fig. 2 illustrates the cross-sections of thin-walled structures: single-wall cylinder, spider web and simplified hedgehog spine, and a quarter section of the bulkheaded hedgehog spine thin-walled structure. The latter three thin-walled structures have different internal structures, and their outer walls are a single-wall cylinder (Fig. 2(a)). The internal structures of the spider web and hedgehog spine structures have 6 ribs (Fig. 2(b)) and 22 ribs (Fig. 2(c) and (d)), respectively, the same as the natural biological structures. The outer wall of the hedgehog spine structure is connected to the ribs by an arc transition that is tangential to both adjacent ribs as well as to the outer wall. Based on the simplified hedgehog spine thin-walled structure, according to the axial characteristics of the real hedgehog spine [24], evenly distributed bulkheads are added within the inner wall and between the inner and outer walls respectively to obtain the bulkheaded hedgehog spine thin-walled structure (Fig. 2(d)). The thicknesses of the bulkheads in the inner wall and between the double walls are 0.78 mm and 0.26 mm, respectively, and the spacings are 5.00 mm and 1.67 mm, respectively (Table 1). The thicknesses of the two kinds of bulkheads at the end surface of the structure are 0.39 mm and 0.13 mm, respectively, only 1/2 of those in the middle. For the four thin-walled structures, the axial height is 60.0 mm, the outer diameter of the outer wall is 30.0 mm, the outer diameter of the inner wall circle or the diameter of the regular hexagonal outer circle is 15.6 mm, and the thickness of the inner walls, the outer walls, and the ribs is 0.6 mm (Table 2).

2.2. Sample preparation and quasi-static uniaxial crushing experiment

The three thin-walled samples of single-wall cylinder, spider web and simplified hedgehog spine (Fig. 3(a)) were prepared with a 3D metal printer EP-250 with printing accuracy of 0.02 mm by using Selective Laser Melting technology. The printing material is aluminum

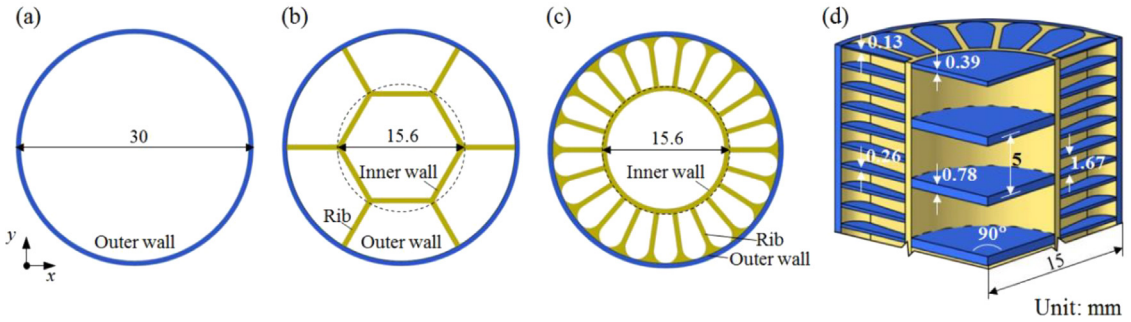

Fig. 2. Cross sections of single-wall cylinder (a), spider web (b), and simplified hedgehog spine (c) thin-walled structures, and a quarter section of the bulkheaded hedgehog spine thin-walled structure (d).

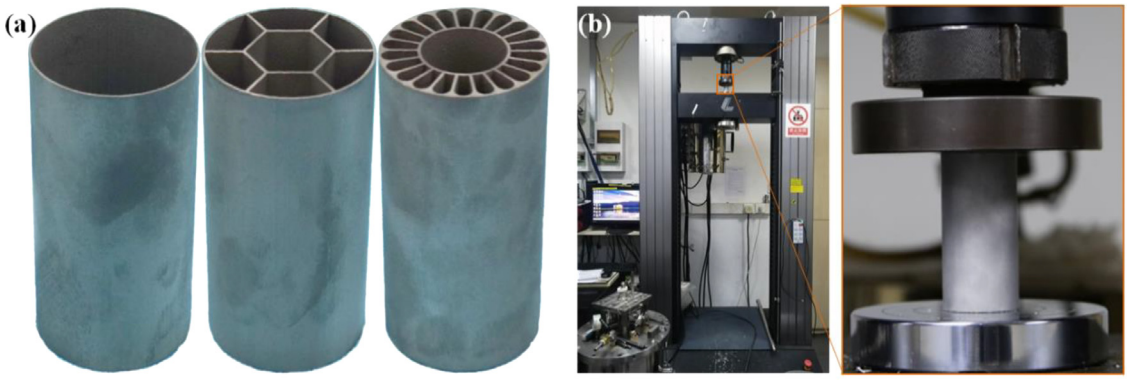

Fig. 3. Thin-walled specimens (a) and quasi-static compression test (b).

Table 1
Thickness and spacing of the bulkheads.

Bulkheads in the inner wall		Bulkheads between the double walls	
Thicknesses (mm)	Spacing (mm)	Thicknesses (mm)	Spacing (mm)
0.78	5	0.26	1.67

Table 2
Global dimensions of the four thin-walled structures.

Height (mm)	Outer diameter (mm)		Thickness (mm)
	Outer wall	Inner wall	Walls and ribs
60.00	30.00	15.60	0.60

alloy AlSi10Mg powder, which is easily castable metal additive manufacturing base material powder of low density and high strength. The main printing parameters are as follows: laser power of 200 W, scanning speed of 8 m/s and layer thickness of 30 um. According to ASTM E9-2009 standard, quasi-static compression tests were carried out on the samples using a LE5105 testing machine, and the moving downward speed of the upper plate was 3 mm/min with a maximum displacement of 50 mm (Fig. 3(b)). The maximum load of the testing machine is 100 kN. When the test load is less than 1/100 of the sensor range, the test accuracy is ± 0.5%. Before loading, the central axis of the sample passes through the center of the upper plate and the support on the testing machine. The upper plate of the testing machine was adjusted to be nearly in contact with the top face of the sample, and displacement and force sensors were reset to zero. At the same time, the height and angle of the camera were adjusted so that the central axis of the lens is perpendicular to the axial section of the sample and is located at the same height as the center of the sample. During loading, the displacement sensor's reading of the testing machine is the displacement of the upper plate, the force sensor's reading is the force borne by the sample, and the sampling frame frequency was 10 s^{-1}. Three tests were conducted for each structure.

2.3. Finite element simulation of quasi-static and dynamic impact crushing process

The quasi-static and dynamic impact compression processes of thin-walled structures were simulated using finite element software ABAQUS (Fig. 4). Based on the element size convergence results, C3D8R was generated by sweep mesh technique with element sizes of 0.3 mm, and the element numbers of single-wall cylinder, spider web, simplified hedgehog spine and bulkheaded hedgehog spine samples were 137,400, 240,000, 516,800 and 773,407, respectively.

An elastic–plastic constitutive model was adopted, and the density of 2.7 g/cm^3, elastic modulus of 72 GPa, Poisson's ratio 0.33, yield strength of 260 MPa and tensile strength of 390 MPa of AlSi10Mg were input. Ignoring the strain rate effect of aluminum alloy materials [21,25,29]. The failure and deletion of an element was simulated by the ductile fracture failure criterion. The equivalent strain was defined as $\sqrt{2[(\varepsilon_1-\varepsilon_2)^2+(\varepsilon_2-\varepsilon_3)^2+(\varepsilon_3-\varepsilon_1)^2]/9}$, where ε_1, ε_2 and ε_3 are the three principle strains. When the material reaches the yield strength, plastic deformation begins to occur. With the continuous accumulation of plastic deformation, damage initiation occurs when the equivalent strain of a certain element reached the measured fracture strain value 0.8, and the accumulated equivalent plastic strain is equal to 0.075. Then the damage accumulates and the element is deleted when the given failure displacement of 0.02 mm is reached.

In the modeling process, the axis of the thin-walled structure is perpendicular to the support, and its axis passes through the center of the support. In the case of quasi-static compression, the bottom surface of the structure is contact with the surface of the support. The included angle between the upper plate and the horizontal direction is $\theta = 0°$, the loading rate is $v = 3$ mm/min and the maximum crushing displacement in the z direction is 50 mm. In the case of

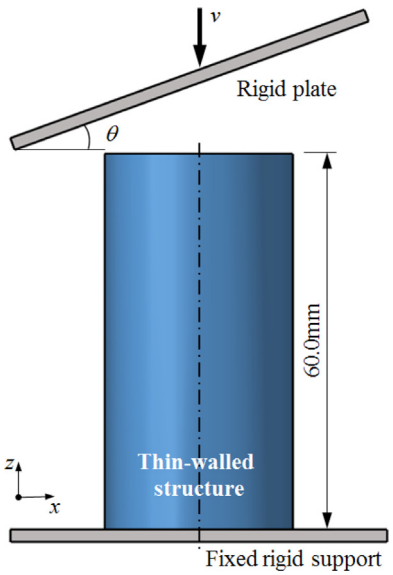

Fig. 4. Diagram of quasi-static and dynamic impact compression thin-walled structures.

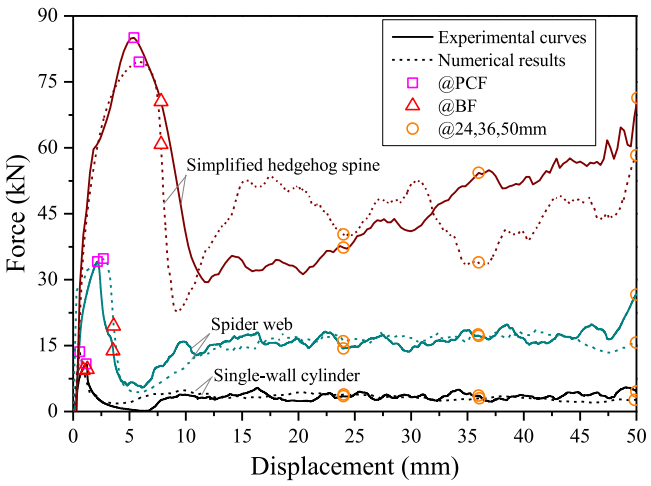

Fig. 5. Force–displacement curves of thin-walled structures under quasi-static compression with speed of 3 mm/min.

impact compression, the bottom surface of the structure is bound with the surface of the support to prevent the sample from sliding along the horizontal direction under the oblique impact load. The included angles between the upper plate and the horizontal direction are θ = 0°, 10°, 20° and 30°, the impact speed is v = 10 m/s. According to the "Test Method for Collapse of Automotive Energy Absorbing Box Components" provided by the Chinese Society of Automotive Engineering [30] and existing reports on crashworthiness of thin-walled structures [11,26,29], the ratio of maximum crushing displacement to sample height is about 0.6, the maximum crushing displacement in the z direction was determined to be 60 mm × 0.6 = 36 mm. Rigid body models were adopted for the upper plate and support. All degrees of freedom of the upper plate except the z direction were constrained, and the support was completely fixed. Furthermore, in order to avoid unexpected penetration, self-contact was defined in areas where contact may occur. All contact areas are set with hard contact along the normal direction of the surface and surface friction along the tangent direction, and the friction coefficient is 0.1.

3. Results and discussions

3.1. Quasi-static compression experiment and simulation

Fig. 5 shows the force–displacement curves of single-wall cylinder, spider web and simplified hedgehog spine thin-walled structures under quasi-static compression. It can be seen that the finite element simulation results of the crushing force–displacement curves are basically consistent with the contour and maximum value of the experimental curves. The crushing force–displacement curves of the three samples all showed a sharp increase at the initial stage, until the crushing force reached the peak, then dropped rapidly, and finally entered the platform fluctuation stage. Based on the crushing force–displacement curve, the integral area under the curve corresponding to the crushing displacement of 50 mm was calculated, and the energy absorbed by the three samples was obtained. Among them, the experimental values are 185.4 J, 803.1 J and 2343.7 J, respectively, and the simulated values are 183.9 J, 795.6 J and 2408.7 J, respectively, with the relative deviation of less than 3% from the experimental values.

Fig. 6 shows the configurations of three thin-walled structures during quasi-static compression at five characteristic moments, namely, the peak crushing force (□ in Fig. 5), the moment before element failure (△ in Fig. 5), and the crushing displacement of 24.0 mm, 36.0 mm and 50.0 mm respectively (∘ in Fig. 5). The single-wall cylinder and spider web thin-walled structures present a curling fracture mode. At the initial stage of compression, the crushing force increases continuously until one end of the cylinder wall buckles, and the crushing force reaches its peak. With element failure occurring at the buckling area, the crushing force decreases continuously. Then curl fracture gradually spreading to the other end, the crushing force enter the platform fluctuation until the whole structure collapses (Figs. 5 and 6(a)–(b)). The simplified hedgehog spine thin-walled structure presents an expansion fracture mode (Figs. 5 and 6(c)). At the initial stage of compression, the crushing force increases continuously until the middle part of the cylinder wall expands unevenly transversely and the crushing force reaches its peak. As the expanding area produces transverse cracks and fracture, the crushing force decreases continuously. Subsequently, the end part of the sample collapses and folds, leading to the slow increase in the crushing force. It can be seen that the configurations of the three thin-walled structures obtained by finite element simulation during quasi-static compression are in good agreement with the experimental configurations.

Therefore, in the case of quasi-static compression, the finite element simulation results and the experimental results have a high degree of agreement for the force–displacement curve characteristics, the value of absorbed energy, the compression process and the final collapse morphology, which verifies the effectiveness of the finite element simulation in this paper.

3.2. Crashworthiness of thin-walled structures

Fig. 7 shows the crushing force–displacement curves of four thin-walled structures under dynamic impact compression. It can be seen from all such crushing force–displacement curves that the crushing force declines to varying degrees after reaching the peak, and finally enters the fluctuating platform stage; both the peak value and fluctuating platform of the crushing force decline with the increase of impact angle.

The parameters for quantitative characterization of the crashworthiness of thin-walled structures, namely specific energy absorption (*SEA*), mean crushing force (*MCF*), peak crushing force (*PCF*) and crushing force efficiency (*CFE*), can be obtained based on the crushing force–displacement curves [26,29]. The energy absorbed by a thin-walled structure corresponding to a certain crushing displacement can be obtained by calculating the area integral of the crushing force–displacement curve concerned within the interval from 0 to the certain crushing displacement. The energy absorbed by a unit structure mass,

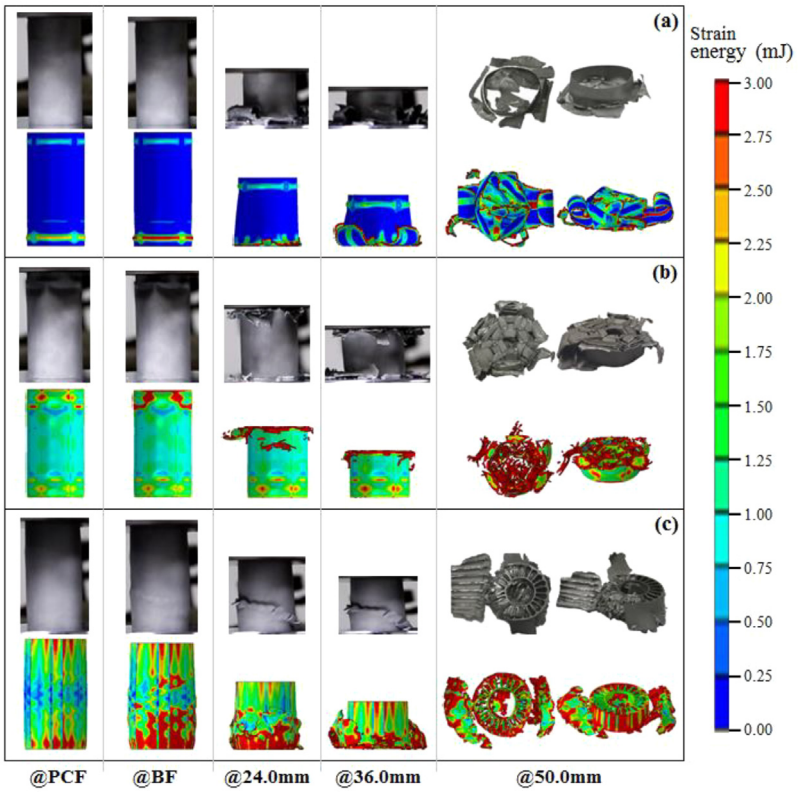

Fig. 6. Configuration evolution of thin-walled structures during quasi-static compression. (a) Single-wall cylinder; (b) Spider web; (c) Simplified hedgehog spine. For each structure, the first and second rows are the experimental and simulation results, respectively.

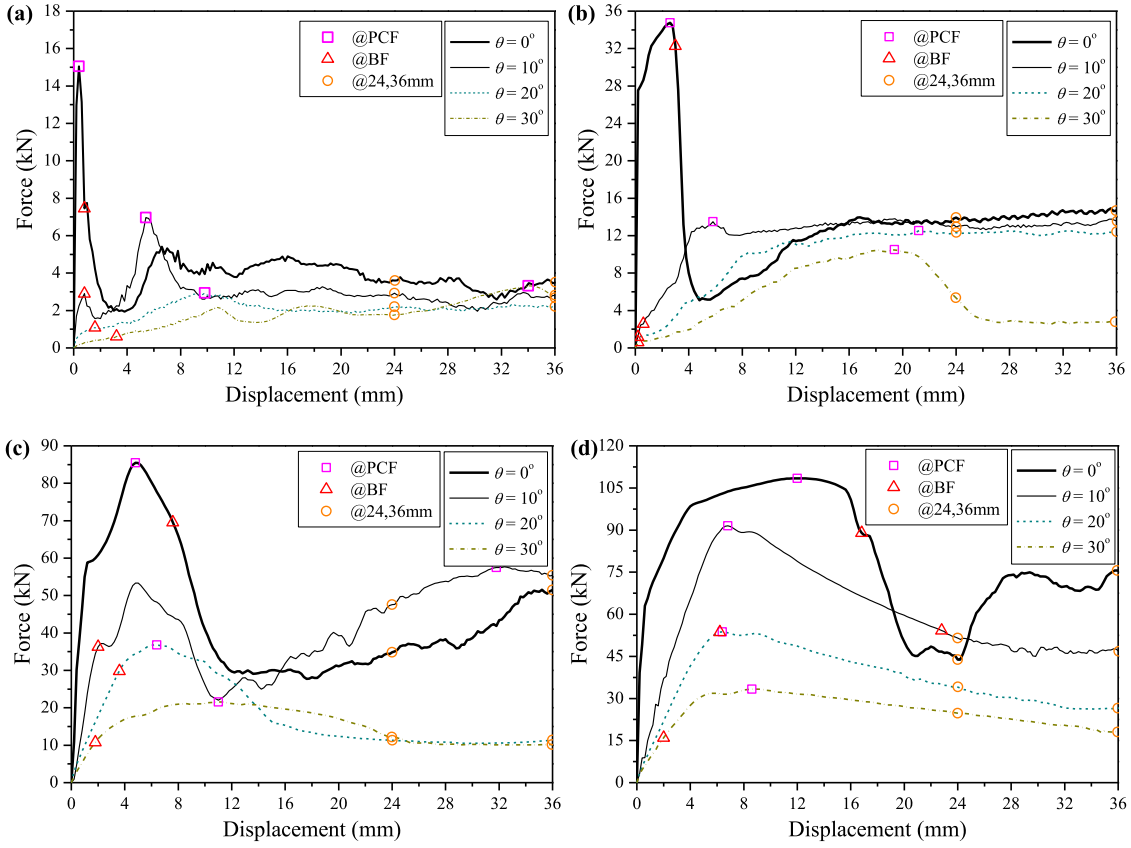

Fig. 7. Force–displacement curves of thin-walled structures under dynamic impact compression. (a) Single-wall cylinder; (b) Spider web; (c) Simplified hedgehog spine; (d) Bulkheaded hedgehog spine.

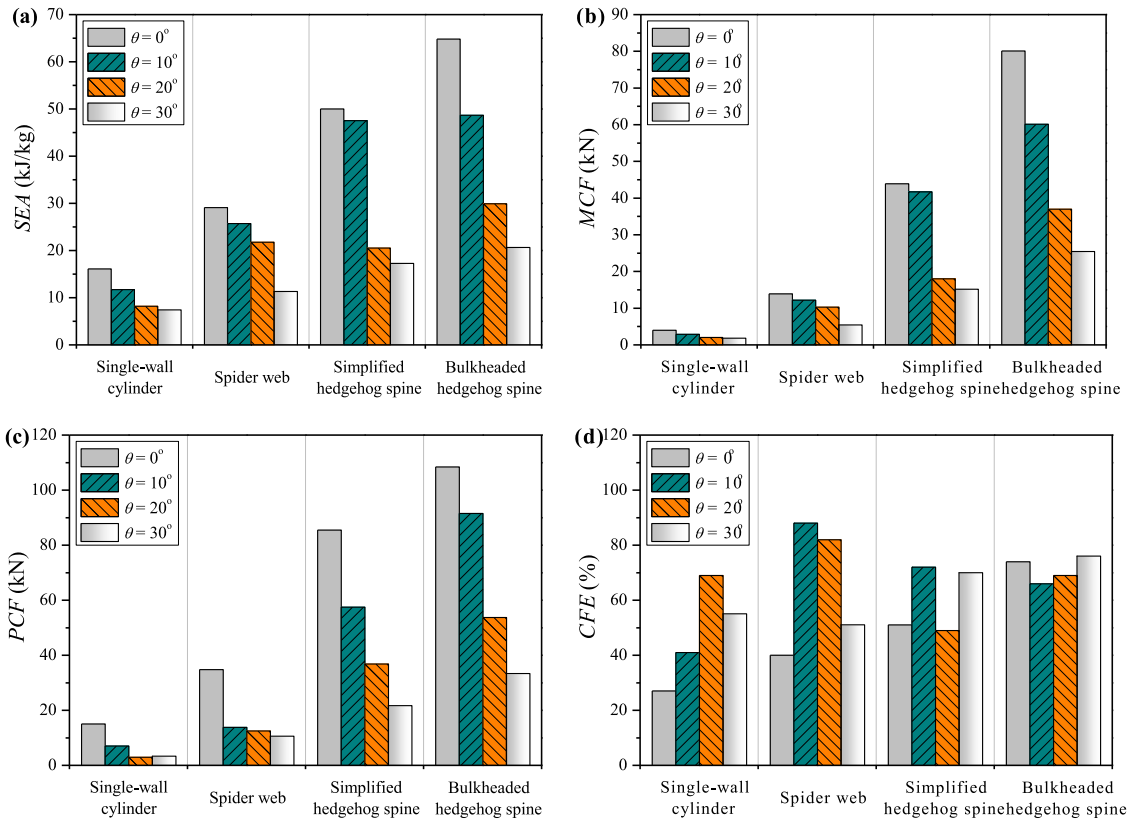

Fig. 8. Crashworthiness of thin-walled structures with crushing displacement of 36 mm. (a) Specific energy absorption; (b) Mean crushing force; (c) Peak crushing force; (d) Crushing force efficiency.

namely *SEA*, can be obtained by dividing the total energy absorbed by the structure by the mass of the structure. The average force of the structure in the process of fold formation, namely *MCF*, can be obtained by dividing the total energy absorbed by the crushing displacement. The maximum value of crushing force in the process of impact and the ratio of mean crushing force to peak crushing force are referred to as *PCF* and *CFE*, respectively.

All the three crashworthiness indicators of the four thin-walled structures, namely *SEA*, *MCF* and *PCF*, decrease with the increase of impact angle, and those of the bulkheaded hedgehog spine thin-walled structure are the highest at each impact angle (Fig. 8(a)–(c)). Under axial impact, the *SEA* of bulkheaded hedgehog spine thin-walled structure is 4.0, 2.2 and 1.3 times that of single-wall cylinder, spider web and simplified hedgehog spine thin-walled structures, the *MCF* is 20.0, 5.8 and 1.8 times that of the three structures, and the *PCF* is 7.2, 3.1 and 1.3 times that of the three structures. Under oblique impact, the *SEA* of the bulkheaded hedgehog spine thin-walled structure is 4.1, 1.9 and 1.5 times at most that of single-wall cylinder, spider web and simplified hedgehog spine thin-walled structures, the *MCF* is 20.7, 4.9 and 1.7 times at most that of the three structures, and the *PCF* is 18.5, 6.6 and 1.6 times at most that of the three structures, respectively. Obviously, under the compression of axial or oblique impact, the bulkhead-based hedgehog spine design can significantly increase the *MCF* of thin-walled structure to obtain the maximum *SEA*, while effectively avoiding the potential damage of impact acceleration arising from excessively high *PCF* to drivers.

Under the compression of axial and oblique impacts, the *CFE* of the bulkheaded hedgehog spine thin-walled structure is 71% ± 5%, indicating that the value is higher and fluctuates more slightly with the change of impact angle, while the *CFE* of the other three thin-walled structures fluctuate more violently as the impact angle changes (Fig. 8(d)). At the same impact angle, the *CFE* of the bulkheaded hedgehog spine thin-walled structure is higher than that of single-wall cylinder and simplified hedgehog spine thin-walled structures, respectively 2.7 and 1.5 times that of the latter two structures under axial impact, and 1.6 and 1.4 times at most under oblique impact. The *CFE* of the spider web thin-walled structure is 65% ± 23%, fluctuating most violently with the change of impact angle among the four structures. As compared with bulkheaded hedgehog spine thin-walled structure, the *CFE* of the spider web thin-walled structure is lower under axial impact or at the impact angle of 30°, though higher at the impact angle of 10° or 20°. In other words, the bulkheaded hedgehog spine thin-walled structure can maintain a high and stable *CFE* at different impact angles, indicating that compared with the other three structures, such structure shows better crushing force uniformity and more uniform deformation.

Ingenious bionic structure designs can significantly improve the crashworthiness of thin-walled structures under axial or oblique impact. Among the four thin-walled structures introduced in this paper, the bulkheaded hedgehog spine thin-walled structure performs best in bearing and energy absorption, much better than the other three structures, followed by the simplified hedgehog spine, spider web and single-wall cylinder thin-walled structures in sequence.

3.3. Configuration evolution under impact compression

The failure modes of the four thin-walled structures under axial impact compression are similar with those under quasi-statistic axial compression. Specifically, the single-wall cylinder and spider web thin-walled structures both present the failure mode of curling fracture (Figs. 9(a) and 10(a)), in which the upper end of cylinder wall first curls to fracture and the fracture gradually spreads downward, finally making the upper part of the structures crushed and failed. The fractured cylinder walls of the aforesaid two structures respectively present larger petal-like curls and smaller sliver-like curls. The simplified hedgehog spine thin-walled structure presents the failure mode of expansion fracture (Fig. 11(a)), with the fractured end parts of the cylinder wall

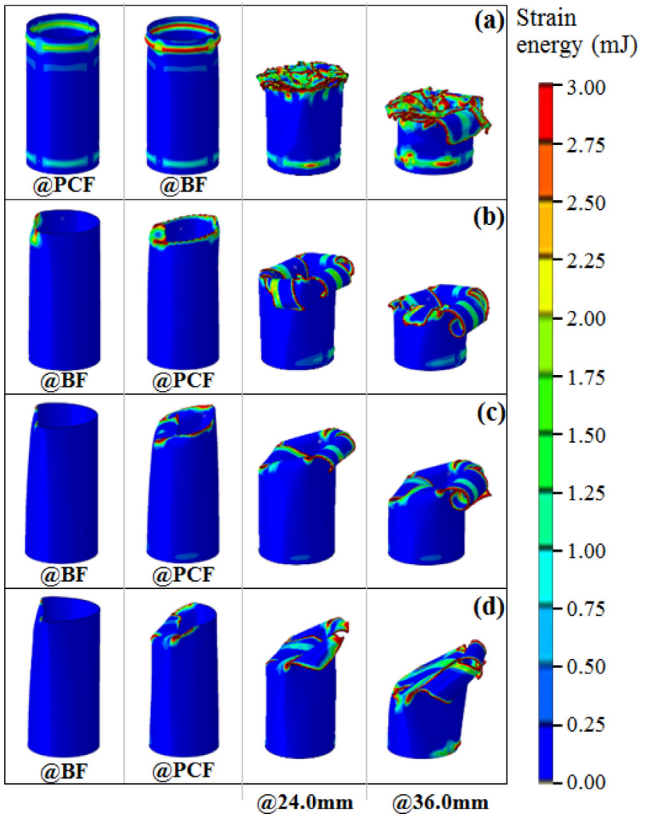

Fig. 9. Configuration and strain energy distribution evolution of single-wall cylinder during impact compression. The impact angles are 0° (a), 10° (b), 20° (c), and 30° (d), respectively.

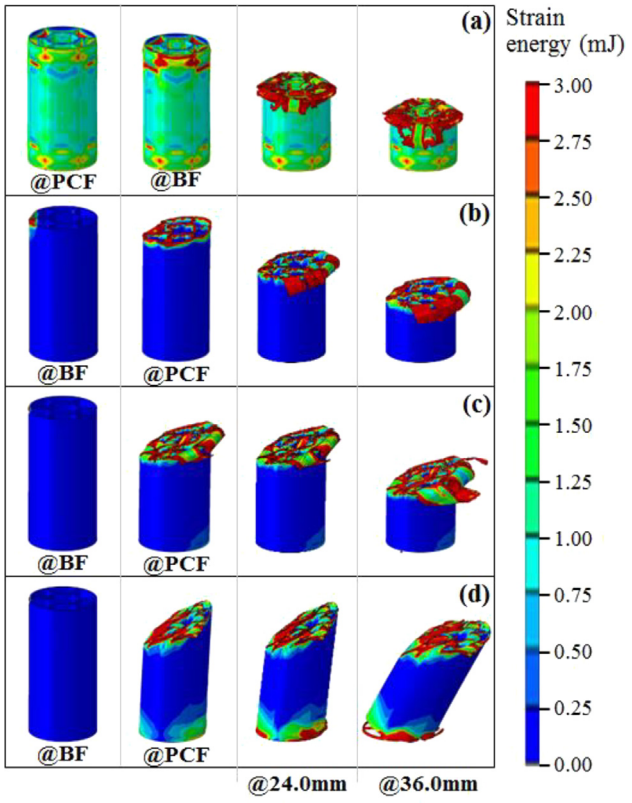

Fig. 10. Configuration and strain energy distribution evolution of spider web thin-walled structure during impact compression. The impact angles are 0° (a), 10° (b), 20° (c), and 30° (d), respectively.

crushed and folded after the middle part thereof expands to fracture. The bulkheaded hedgehog spine thin-walled structure presents the failure mode of expansion-shear fracture (Figs. 7(d) and 12(a)). At the initial stage of compression, the lateral expansion of cylinder body is more uniform than that of the simplified hedgehog spine thin-walled structure, the crushing force constantly increased until reaching the peak. After shear fracture occurs at the end parts of the cylinder wall, the crushing force decreases continuously. Finally, the fractured parts squeeze each other, causing the crushing force to rise significantly.

Under oblique impact, the structures withstand axial pressure and shear force simultaneously, with the plate firstly contacting a side of the sample top and the part of cylinder wall in the contact area being pressed. At a smaller impact angle, in the contact area of single-wall cylinder (Figs. 7(a) and 9(b)–(c)) or spider web (Figs. 7(b) and 10(b)–(c)) thin-walled structures, the cylinder wall curls inwards the structure until element failure occurs and the cylinder wall fractures with the crushing force reaches the peak. Then the part of cylinder wall at the side far from the flat panel curls and fractures outwards, resulting in a decrease in the crushing force of the single-wall cylinder. Under the action of ribs, the crushing force of the spider web directly enters platform fluctuation stage. Finally, the upper part of the two structures curls to fracture, with the curling degree of cylinder wall featuring petal-like or sliver-like fracture higher than that under axial impact. In the contact area of the simplified hedgehog spine thin-walled structure (Figs. 7(c) and 11(b)), the cylinder wall collapses inwards and element failure occurs with the crushing force reaches the peak. Then the cylinder body in the contact area is gradually crushed axially leading crushing force decreases. With the part thereof at the side far from the flat panel separated after being sheared to fracture, and the inner wall curling inwards and the ribs and outer wall curling outwards respectively without any folding, the crushing force continues to rise.

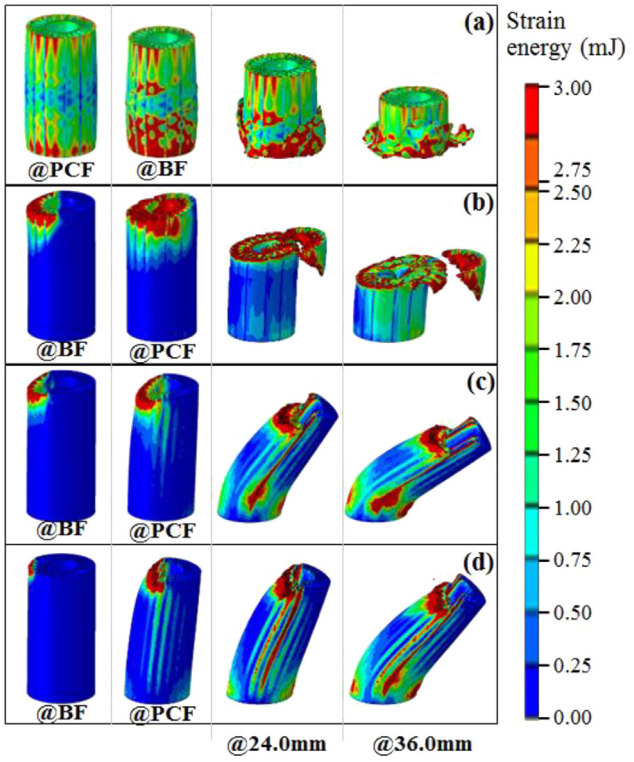

Fig. 11. Configuration and strain energy distribution evolution of simplified hedgehog spine thin-walled structure during impact compression. The impact angles are 0° (a), 10° (b), 20° (c), and 30°(d), respectively.

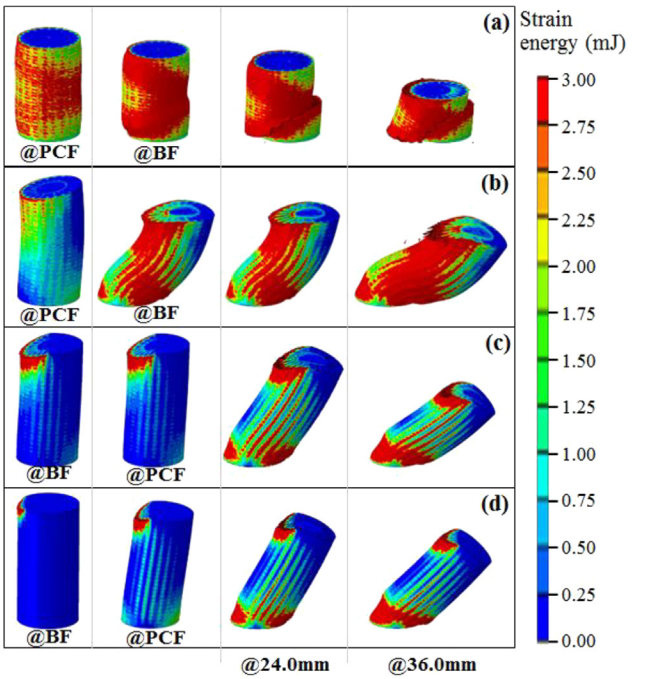

Fig. 12. Configuration and strain energy distribution evolution of bulkheaded hedgehog spine thin-walled structure during impact compression. The impact angles are 0° (a), 10° (b), 20° (c), and 30°(d), respectively.

The bulkheaded hedgehog spine thin-walled structure slightly obliques and bends overall (Figs. 7(d) and 12(b)), the crushing force reaches the peak. With the bottom part of cylinder body at the side far from the flat panel being pressed until element failure occurs, followed by more severe compression deformation in this area and finally overall buckling, the crushing force reduces linearly.

At a larger impact angle, for single-wall cylinder (Figs. 7(a) and 9(d)) or spider web (Figs. 7(b) and 10(d)) thin-walled structures, the part of cylinder wall in the contact area and that at the side far from the plate curl to fracture to varying degrees. The bottom of the single-wall cylinder is local buckling, and the crushing force has no significant change. While the bottom of the spider web thin-walled structure breaks and causes the cylinder overall obliqueness, which greatly reduce the crushing force after the peak. The part of cylinder wall in the contact area of the simplified hedgehog spine thin-walled structure collapses inwards (Figs. 7(c) and 11(c)–(d)), followed by local buckling at the sample bottom before gradual crushing of the cylinder body and significant obliqueness of the two parts that the cylinder body is axially sheared into, which makes the crushing force decrease and enter the platform stage. In the contact area of the bulkheaded hedgehog spine thin-walled structure (Figs. 7(d) and 12(c)–(d)), the cylinder body also collapses inwards and element failure occurs, and then the cylinder body slightly obliques, with the bottom part of cylinder body at the side far from the flat panel being pressed, accompanied by element failure and local buckling, making the structure significantly oblique without any overall fracture failure, leading to the crushing force to reach the peak and then reduce slowly.

The configuration evolution modes of the four thin-walled structures can significantly affect the crashworthiness thereof at each impact angle. With poor constraint capability, the cylinder wall of the single-wall cylinder structure curls to fracture in large area in the process of compression deformation, and thus fails to continuously participate in bearing, making the single-wall cylinder structure least crashworthy, seconded by the spider web thin-walled structure, whose cylinder wall has mitigated degree of curling to fracture thanks to the enhanced constraint due to additional inner wall and ribs. With further enhanced constraint capability, the cylinder wall of the simplified hedgehog spine thin-walled structure can continue to participate in bearing even after fracture, making it more crashworthy than the aforesaid two structures. With its cylinder wall being free of curling or axial fracture, the bulkheaded hedgehog spine thin-walled structure can participate in bearing as a whole, and thus has the best crashworthiness. Under oblique impact, especially in case of large impact angles, the cylinder wall fracture and failure mode of the four thin-walled structures may be gradually transformed into overall obliqueness arising from local buckling, accompanied by greatly reduced bearing capacity, making the crashworthiness of these structures under oblique impact than that under axial impact.

3.4. Comparative analysis for collapse modes

Geometrical configuration can significantly affect the failure mode of thin-walled structures under impact compression. The cylindrical area within the outer wall of thin-walled structures may be divided into multiple unconnected cavities by the inner wall, ribs, bulkheads or others. The smaller the cavities are, the less likely the cylinder wall is to undergo local buckling, and the earlier the contact between different parts of the cylinder wall will take place in the process of folding or curling, which can restrain deformation. The stronger the structures' resistance against deformation is, the shorter the folding wavelength will be.

Fig. 13 shows the axial profiles of the four thin-walled structures, representing the folding or curling form of the cylinder wall thereof at the crushing displacement of 36 mm. In the process of impact compression, the thin-walled structures gradually collapse with the cylinder wall thereof gradually folding or curling. The point with the smallest curvature radius of bending on the cylinder wall is referred to as a plastic hinge, and the linear distance between two adjacent plastic hinges is denoted as folding wavelength [13,25]. Premised on the same crushing displacement, the shorter the folding wavelength is, the more plastic hinges are formed per unit length of the axial section of the cylinder wall. The more uniform the deformation of the thin-walled structure is, and the more material is involved in deformation.

Among the four thin-walled structures, the single-wall cylinder structure has the largest axial run-through cavities. Under axial or oblique impact, the upper half of the cylinder wall freely curls in the cavities, without restraining deformation, leading to the longest folding wavelength and the poorest bearing and energy absorption performance. As the impact angle increases, the folding wavelength increases, and less material is involved in deformation. Besides, at a larger impact angle, the cylinder body may tilt slightly, thus resulting in the decrease of *MCF* and *SEA* (Fig. 13(a)).

The cylinder cross section of the spider web thin-walled structure is divided into a hexagon combines with multiple fan-shaped sections by the inner wall and ribs of the structure. The upper half of the cylinder wall mainly curls in smaller axially run-through cavities, leading to enhanced constraint of the cylinder wall and second longest folding wavelength, making the spider web thin-walled structure more crashworthy than the single-wall structure at the same impact angle. As the impact angle increases, the folding wavelength increases, and the *MCF* and *SEA* decrease. Besides, at a larger impact angle, local buckling at the bottom and significant obliqueness of the structure occur, thus resulting in a significant decrease of *MCF* and *SEA* (Fig. 13(b)).

The cross section of the inner wall of the simplified hedgehog spine thin-walled structure is circular and has more ribs. The ribs are connected with the outer wall of the structure through transitional arcs, and the arc is simultaneously tangent to the adjacent two ribs and the outer wall. The annular section between the inner and outer cylinder walls is divided into smaller hammer-shaped sections, the axially run-through cavities are further downsized, and the constraint of the cylinder wall is further enhanced, thus shortening the folding wavelength of the lower half of folded cylinder wall under axial impact

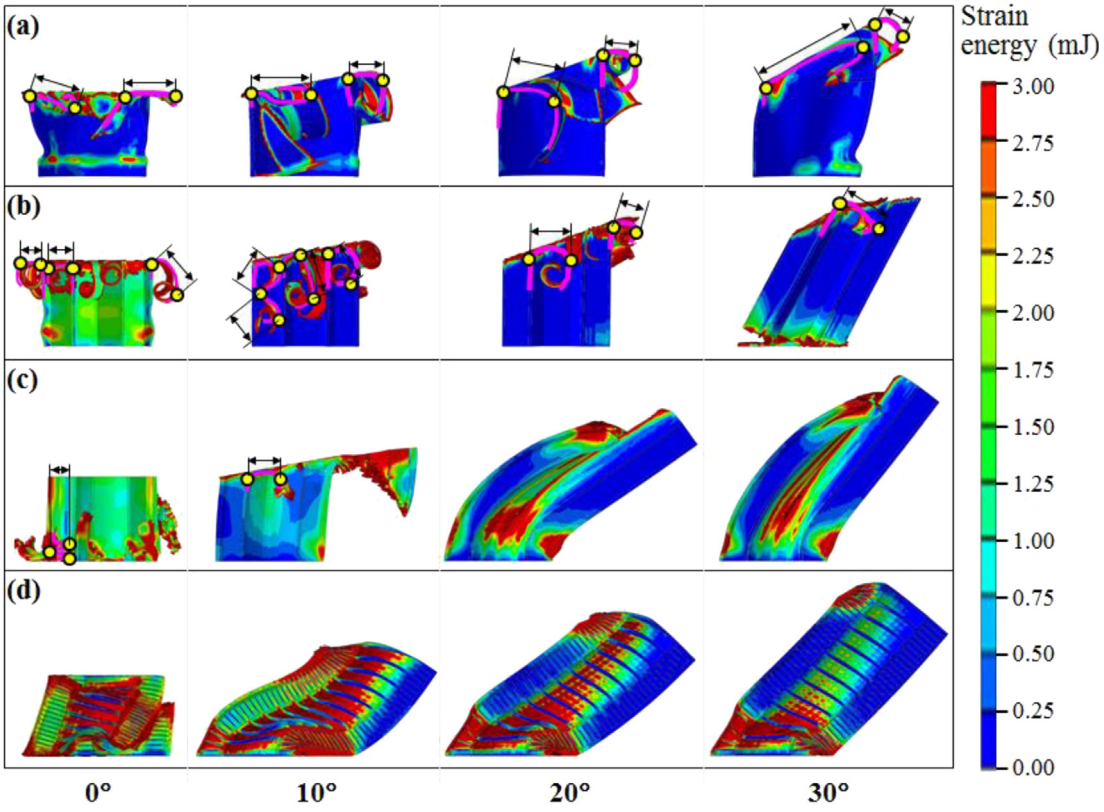

Fig. 13. Axial profiles of the thin-walled structures with crushing displacement of 36 mm. (a) Single-wall cylinder; (b) Spider web; (c) Simplified hedgehog spine; (d) Bulkheaded hedgehog spine. Where, the yellow circles represent the plastic hinge, and the linear distance between two adjacent plastic hinges is the folding wavelength.

and the curled inner wall under oblique impact at a small angle, making the simplified hedgehog spine thin-walled structure more crashworthy than the aforesaid two structures. At larger impact angles, no folding or curling occurs after the upper cylinder wall collapses inwards, while the cylinder body is axially sheared to fracture, followed by buckling at the bottom and significant obliqueness of the structure as a whole, resulting in a significant decrease of *MCF* and *SEA* (Fig. 13(c)).

Lateral bulkheads are added to the bulkheaded hedgehog spine thin-walled structure, which further divide the hammer-shaped axially run-through cavities between the inner and outer walls and the columnar axially run-through cavity within the inner wall into smaller closed cavities, thus preventing the cylinder wall from folding or curling. Under axial impact, the sample presents more uniform expansion, with the two end parts that the cylinder wall is axially sheared and fractured into pressing each other. Under oblique impact, despite buckling at the bottom, the axial shear and fracture identified in the simplified hedgehog spine thin-walled structure can be effectively avoided, thus maintaining good structural integrity. The involvement of more material in bearing against deformation makes the *MCF* and *SEA* of the bulkheaded hedgehog spine thin-walled structure gradually decrease with the increase of impact angle, but still much higher than those of the other three structures (Fig. 13(d)).

3.5. Strain energy analysis

During the impact process, the energy absorbed by the thin-walled structure is mainly stored in the form of strain energy and the rest of the energy is dissipated as kinetic energy and friction energy. The strain energy stored in the four thin-walled structures and their internal components under the crushing displacement of 36 mm was calculated and divided by the mass of the structure to obtain the strain energy–mass ratio of the whole structure and its components. Similar to *SEA*, with the increase of impact angle, the strain energy–mass ratio of the four thin-walled structures and their components decreases, but at all impact angles, the strain energy–mass ratio of the bulkheaded hedgehog spine thin-walled structure is the highest among the four structures (Fig. 14).

The strain energy–mass ratio of bulkheaded hedgehog spine thin-walled structure under axial impact is 4.5, 2.8 and 1.4 times that of single-wall cylinder, spider web and simplified hedgehog spine thin-walled structures, and is 4.6, 2.3 and 1.5 times at most that of the three thin-walled structures respectively under oblique impact (Fig. 14(a)). The single-wall cylinder only has the outer wall. Under different impact angles, the strain energy–mass ratio of outer wall of spider web, simplified hedgehog spine and bulkheaded hedgehog spine thin-walled structures are similar to that of the single-wall cylinder, but their percentages of the strain energy–mass ratio of the corresponding structure decrease in turn, i.e., 52%, 39% and 28%, respectively (Fig. 14(b)). Except for single-wall cylinder, the three structures all contain inner wall and ribs. Under all impact angles, the strain energy–mass ratio of the inner wall and ribs of the bulkheaded hedgehog spine thin-walled structure is the highest, which is 3.1 and 1.3 times that of spider web and simplified hedgehog spine thin-walled structures under axial impact, and is 2.8 and 1.3 times at most that of these two structures under oblique impact, respectively (Fig. 14(c)). In addition, the strain energy–mass ratio of the bulkheads of bulkheaded hedgehog spine is slightly lower than its outer wall and far lower than that of its inner wall and ribs (Fig. 14(d)). Therefore, different configuration design has little influence on the energy storage performance of the outer wall of thin-walled structures, but has significant influence on the energy storage performance of the inner wall and other components. The design of inner wall and rib of hedgehog spine makes the strain energy–mass ratio of the inner wall and ribs of two hedgehog spine thin-walled structures is higher than that of the spider web thin-walled structure. The bulkhead plays a weak role in deformation energy storage and mainly improves the energy storage performance of the inner wall and ribs component.

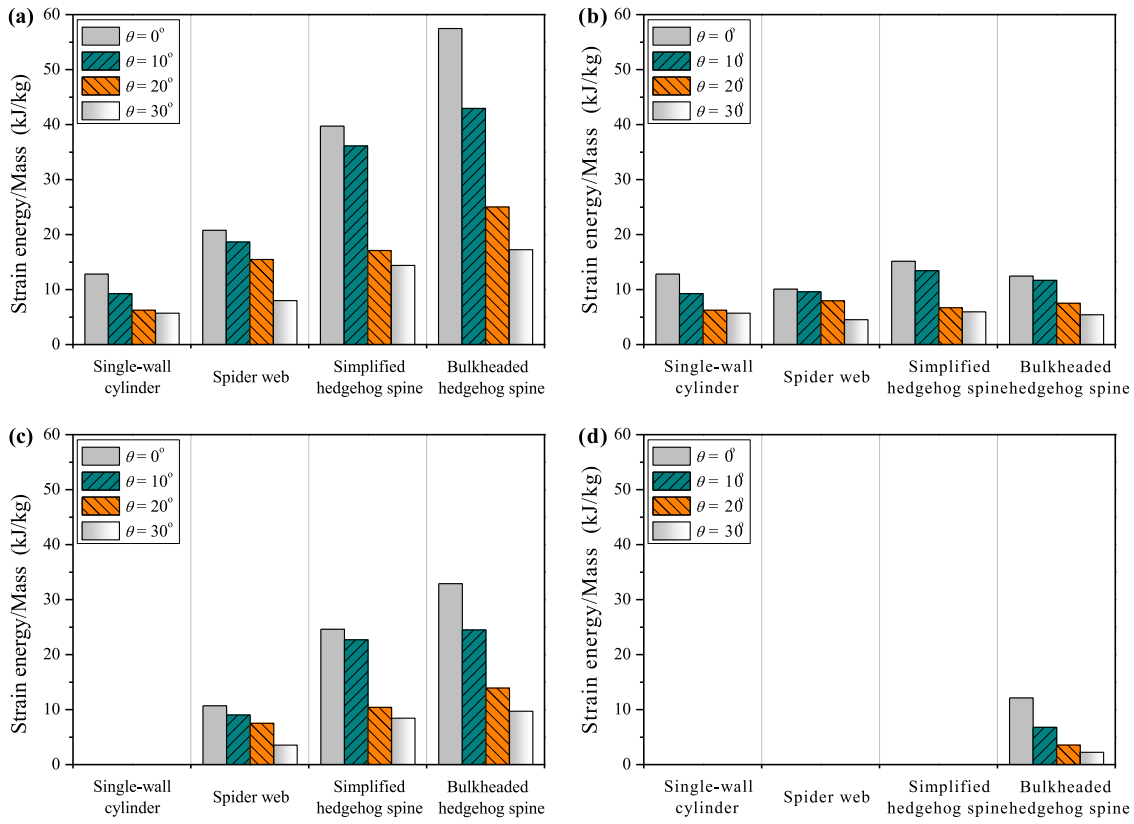

Fig. 14. Strain energy/Mass of thin-walled structure and its components with crushing displacement of 36 mm. (a) Whole structure; (b) Outer wall; (c) Inner wall and ribs; (d) Bulkheads.

Fig. 15 shows the strain energy distribution of the four thin-walled structures along the axial direction with crushing displacement of 36 mm. Divide the structure along the axis into 30 equal parts. For each equal part, count the sum of strain energy of all elements in each structure, and divide the sum by the mass of the equal part to get the strain energy per unit mass of each equal part. The normalized position coordinates are obtained by dividing the axial distance from each equal part midpoint to the upper surface of the structure by the axial height 60 mm.

Under different impact angles, the strain energy per unit mass of the failure regions such as fracture and buckling in the thin-walled structure is higher. With the increase of impact angle, the strain energy per unit mass in failure area decreases. For single-wall cylinder structure, the strain energy per unit mass in failure region is the lowest, and that in other regions is almost 0, indicating the weakest energy absorption performance of the structure (Fig. 15(a)). For spider web thin-walled structure, the strain energy per unit mass in the failure region is higher than that of single-wall cylinder, while the value in other regions is also almost 0, making the energy absorption performance better than that of the single-wall cylinder (Fig. 15(b)). For the simplified hedgehog spine thin-walled structure, the strain energy per unit mass of the failure region under axial and small impact angle is much higher than the previous two structures, which makes the energy absorption performance higher. However, the strain energy per unit mass of failure region under larger impact angles is similar to that of the spider web thin-walled structure, while that of other regions is relatively low, resulting in a significant reduction in energy absorption performance at these impact angles (Fig. 15(c)). For the bulkheaded hedgehog spine thin-walled structure, the strain energy per unit mass of the failure region under axial and small impact angle is similar to that of the simplified hedgehog spine, and the strain energy per unit mass of other region is much higher than that of single-wall cylinder and spider web thin-walled structures. In addition, the strain energy per unit mass of the failure region under larger impact angles is much higher than that of the other three structures, which makes the bulkheaded hedgehog spine thin-walled structure have the best energy absorption performance under different impact angles (Fig. 15(d)). It can be seen that under axial and oblique impact, the energy storage performance of the failure region of bulkheaded hedgehog spine thin-walled structure is much higher than that of the other three structures, and other areas also play an excellent role in energy storage, indicating that more materials in the structure participate in deformation, thus significantly improving the overall energy absorption capacity.

4. Conclusion

In this paper, the bulkheaded hedgehog spine thin-walled structure is designed by simulating the configuration characteristics of the cross and longitudinal sections of hedgehog spines. Such structure is compared with the single-wall cylinder, spider web and simplified hedgehog spine thin-walled structures in terms of axial and oblique crashworthiness, by using the 3D metal printing technology, the quasi-static compression test and the finite element simulation. In addition, the mechanism for comprehensively improving the crashworthiness of the bulkheaded hedgehog spine thin-walled structure by the configuration design is discussed. The following conclusions can be drawn:

Under axial and oblique impacts, the bulkheaded hedgehog spine thin-walled structure has more material involved in energy storage than the other three structures. In terms of energy storage, the structure's failure area performs better while the other areas also have good performance, which endows the structure with a high specific energy absorption under impact compression, respectively 4.0, 2.2 and 1.3 times that of the other three structures, and 4.1, 1.9 and 1.5 times at most of that of the other three structures under oblique impact.

The bionic configuration design of the bulkheaded hedgehog spine thin-walled structure can, through enhancing the constraint of the

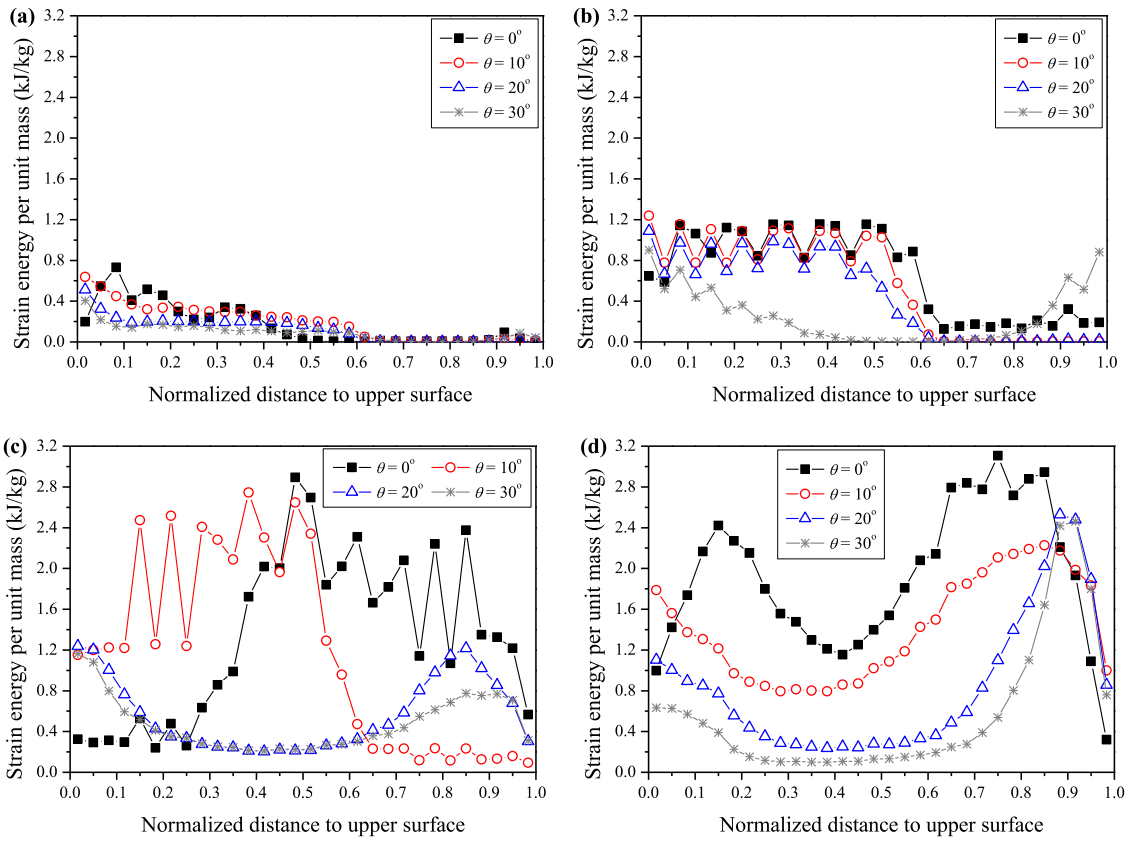

Fig. 15. Distribution of strain energy per unit mass of the thin-walled structure along the axial direction with crushing displacement of 36 mm. (a) Single-wall cylinder; (b) Spider web; (c) Simplified hedgehog spine; (d) Bulkheaded hedgehog spine.

structure's cylinder wall, change the structure's configuration evolution and failure mode in the process of impact compression. Therefore, curling fracture under axial impact and shear fracture under oblique impact can be avoided, demonstrating the structure's great deformation coordination, thus significantly increasing the mean crushing force at different impact angles and achieving high and stable crushing force efficiency.

The bulkheaded hedgehog spine thin-walled structure has better axial and oblique crashworthiness than the existing thin-walled structures. However, it cannot be prepared with the existing 3D printing technology. Therefore, the next step is to continue to improve the configuration on this basis, in order to obtain the thin-walled structure with high crash resistance that can be prepared for practical application.

CRediT authorship contribution statement

Bin Liu: Writing – original draft, Software, Investigation, Data curation. **Xianghong Xu:** Writing – review & editing, Funding acquisition, Conceptualization.

Declaration of competing interest

The authors declare that they have no known competing financial interests or personal relationships that could have appeared to influence the work reported in this paper.

Data availability

Data will be made available on request.

Acknowledgments

The authors gratefully acknowledge the support provided by the National Natural Science Foundation of China (No. 11672297). All authors approved the version of the manuscript to be published.

References

[1] C.W. Isaac, Crashworthiness performance of green composite energy absorbing structure with embedded sensing device providing cleaner environment for sustainable maintenance, Sustain. Mater. Technol. 25 (2020) e00196, http://dx.doi.org/10.1016/j.susmat.2020.e00196.

[2] C.W. Isaac, F. Duddeck, Current trends in additively manufactured (3D printed) energy absorbing structures for crashworthiness application – a review, Virtual Phys. Prototy 17 (4) (2022) 1058–1101, http://dx.doi.org/10.1080/17452759.2022.2074698.

[3] C.Y. Wang, Li. Y., et al., Structure design and multi-objective optimization of a novel crash box based on biomimetic structure, Int. J. Mech. Sci. 138-139 (2018) 489–501, http://dx.doi.org/10.1016/j.ijmecsci.2018.01.032.

[4] C.W. Isaac, Ezekwem. C., A review of the crashworthiness performance of energy absorbing composite structure within the context of materials manufacturing and maintenance for sustainability, Compos. Struct. 257 (2021) 113081, http://dx.doi.org/10.1016/j.compstruct.2020.113081.

[5] J. Tanaskovic, D. Milkovic, et al., Experimental investigations of the shrinking–splitting tube collision energy absorber, Thin-Walled Struct. 86 (2015) 142–147, http://dx.doi.org/10.1016/j.tws.2014.10.007.

[6] Q. Liu, J.B. Ma, et al., Energy absorption of bio-inspired multi-cell CFRP and aluminum square tubes, Compos. Part B: Eng. 121 (2017) 134–144, http://dx.doi.org/10.1016/j.compositesb.2017.03.034.

[7] S.Y. Ji, S.M. Liang, DEM-FEM-MBD coupling analysis of landing process of lunar lander considering landing mode and buffering mechanism, Adv. Space Res. 68 (3) (2021) 1627–1643, http://dx.doi.org/10.1016/j.asr.2021.03.034.

[8] X.F. Yang, J.X. Ma, et al., Crashworthy design and energy absorption mechanisms for helicopter structures: A systematic literature review, Prog. Aerosp. Sci. 114 (2020) 100618, http://dx.doi.org/10.1016/j.paerosci.2020.100618.

[9] A. Siva Kumar, G. Himabindu, et al., Experimental investigations with crush box simulations for different segment cars using LS-DYNA, Int. J. Curr. Eng. Technol. (2) (2014) http://dx.doi.org/10.14741/ijcet/spl.2.2014.127.
[10] B. Ahmad, S. Mustafa, et al., On the crashworthiness performance of thin-walled energy absorbers: Recent advances and future developments, Thin-Walled Struct. 118 (2017) 137–163, http://dx.doi.org/10.1016/j.tws.2017.05.018.
[11] J.F. Song, S.C. Xu, et al., Experiment and numerical simulation study on the bionic tubes with gradient thickness under oblique loading, Thin-Walled Struct. 163 (2021) 107624, http://dx.doi.org/10.1016/j.tws.2021.107624.
[12] A.N. Ali, H.H. Jamal, et al., Comparative analysis of energy absorption and deformations of thin walled tubes with various section geometries, Thin-Walled Struct. 48 (12) (2010) 946–954, http://dx.doi.org/10.1016/j.tws.2010.07.003.
[13] W.Y. Liu, Z.Q. Lin, et al., Dynamic performances of thin-walled tubes with star-shaped cross section under axial impact, Thin-Walled Struct. 100 (2016) 25–37, http://dx.doi.org/10.1016/j.tws.2015.11.016.
[14] S.T. Liu, Z.Q. Tong, et al., Bionic design modification of non-convex multi-corner thin-walled columns for improving energy absorption through adding bulkheads, Thin-Walled Struct. 88 (2015) 70–81, http://dx.doi.org/10.1016/j.tws.2014.11.006.
[15] G.Y. Sun, T. Pang, et al., Parameterization of criss-cross configurations for multiobjective crashworthiness optimization, Int. J. Mech. Sci. 124-125 (2017) 145–157, http://dx.doi.org/10.1016/j.ijmecsci.2017.02.027.
[16] N. Onsalung, C. Thinvongpituk, et al., Impact response of circular aluminum tube filled with polyurethane foam, Mater. Trans. 55 (1) (2014) 207–215, http://dx.doi.org/10.2320/matertrans.M2013293.
[17] J.F. Song, S.C. Xu, et al., Bionic design and multi-objective optimization for variable wall thickness tube inspired bamboo structures, Thin-Walled Struct. 125 (2018) 76–88, http://dx.doi.org/10.1016/j.tws.2018.01.010.
[18] S. Sharifi, M. Shakeri, et al., Experimental investigation of bitubal circular energy absorbers under quasi-static axial load, Thin-Walled Struct. 89 (2015) 42–53, http://dx.doi.org/10.1016/j.tws.2014.12.008.
[19] T. Dirgantara, A. Jusuf, et al., Crashworthiness analysis of foam–filled square column considering strain rate effect of the foam, Thin-Walled Struct. 129 (2018) 365–380, http://dx.doi.org/10.1016/j.tws.2018.04.004.
[20] G. Tarun, S. Dominik, et al., Microimaging-informed continuum micromechanics accurately predicts macroscopic stiffness and strength properties of hierarchical plant culm materials, Mech. Mater. 130 (2019) 39–57, http://dx.doi.org/10.1016/j.mechmat.2019.01.009.
[21] J. Fu, Q. Liu, et al., Design of bionic-bamboo thin-walled structures for energy absorption, Thin-Walled Struct. 135 (2019) 400–413, http://dx.doi.org/10.1016/j.tws.2018.10.003.
[22] K. Eisuke, A. Shoko, et al., Vascular bundle shape in cross-section and relaxation properties of Moso bamboo (Phyllostachys pubescens), Mat. Sci. Eng. C 31 (5) (2011) 1050–1054, http://dx.doi.org/10.1016/j.msec.2011.03.004.
[23] Z.Q. Wei, X.H. Xu, Numerical study on impact resistance of novel multilevel bionic thin-walled structures, J. Mater. Res. Technol. 16 (2022) 1770–1780, http://dx.doi.org/10.1016/j.jmrt.2021.12.105.
[24] B.Swift. Nathan, Hsiung. Bor-Kai, et al., Dynamic impact testing of hedgehog spines using a dual-arm crash pendulum, J. Mech. Behav. Biomed. 61 (2016) 271–282, http://dx.doi.org/10.1016/j.jmbbm.2016.03.019.
[25] Y. Zhang, J. Wang, et al., Crashworthiness of bionic fractal hierarchical structures, Mater. Des. 158 (2018) 147–159, http://dx.doi.org/10.1016/j.matdes.2018.08.028.
[26] H. Huang, S.C. Xu, et al., Crashworthiness analysis and bionic design of multi-cell tubes under axial and oblique impact loads, Thin-Walled Struct. 144 (2019) 106333, http://dx.doi.org/10.1016/j.tws.2019.106333.
[27] N. Qiu, Y.K. Gao, et al., Crashworthiness analysis and design of multi-cell hexagonal columns under multiple loading cases, Finite Elem. Anal. Des. 104 (2015) 89–101, http://dx.doi.org/10.1016/j.finel.2015.06.004.
[28] S. Pirmohammad, Marzdashti.S. Esmaeili, et al., Crushing behavior of new designed multi-cell members subjected to axial and oblique quasi-static loads, Thin-Walled Struct. 108 (2016) 291–304, http://dx.doi.org/10.1016/j.tws.2016.08.023.
[29] Y. Zhang, X. Xu, et al., Crushing analysis for novel bio-inspired hierarchical circular structures subjected to axial load, Int. J. Mech. Sci. 140 (2018) 407–431, http://dx.doi.org/10.1016/j.ijmecsci.2018.03.015.
[30] http://www.sae-china.org/.